Fabrication of Radio-Opaque and Macroporous Injectable Calcium Phosphate Cement

Habib Belaid, Carole Barou, Pierre-Yves Collart Dutilleul, Alban Desoutter, Marilyn Kajdan, Florence Bernex, Raphaël Tétreau, Frédéric Cuisinier, Jonathan Barés, Vincent Huon, et al.

Fabrication of a radio-opaque and macroporous injectable calcium phosphate cement

Habib Belaid[1,2], Carole Barou[1,2,3], Pierre-Yves Collart-Dutilleul[4], Alban Desoutter[4], Marilyn Kajdan[2], Florence Bernex[2,5], Raphaël Tétreau[6], Frédéric Cuisinier[4], Jonathan Barés[7], Vincent Huon[7], Catherine Teyssier[2], David Cornu[1], Vincent Cavaillès[2]*£ and Mikhael Bechelany[1]*£

[1]Institut Européen des Membranes, IEM-UMR 5635, Université Montpellier, CNRS, ENSCM, 34095, Montpellier, France

[2]IRCM, Institut de Recherche en Cancérologie de Montpellier, INSERM U1194, Université Montpellier, Montpellier F-34298, France

[3]Biologics 4 life, 84120 Pertuis, France

[4]Laboratoire de bioingénierie et nanosciences, EA4203, Université de Montpellier, 34193, Montpellier, France

[5]BioCampus, RHEM, Université de Montpellier, CNRS UAR3426, INSERM, F-34298, Montpellier, France.

[6]Service d'Imagerie, Institut régional du Cancer Montpellier, F-34298, Montpellier, France

[7]Laboratoire de Mécanique et Génie Civil, Univ Montpellier, CNRS, 34090, Montpellier, France

* Corresponding authors:

mikhael.bechelany@umontpellier.fr, Phone: +33467149167, Fax: +33467149119

vincent.cavailles@inserm.fr, Phone: +33411283172

£ Co-last authors

KEYWORDS: Calcium phosphate cement, PLGA microspheres, vertebroplasty, radio-opaque, bone metastasis

ABSTRACT

The aim of this work was the development of an injectable radio-opaque and macroporous calcium phosphate cement (CPC) to be used as a bone substitute for the treatment of pathologic vertebrae fractures. A CPC was first rendered radio-opaque by incorporation of zirconium dioxide (ZrO_2). In order to create macroporosity, Poly Lactic-co-Glycolic Acid (PLGA) microspheres around 100 µm were homogeneously incorporated in the CPC as observed by scanning electron microscopy (SEM). Physicochemical analyses by X-ray diffraction and Fourier-transform infrared spectroscopy confirmed the brushite phase of the cement. The mechanical properties of the CPC/PLGA cement containing 30% PLGA (wt/wt) were characterized with a compressive strength of 2 MPa and a Young's modulus of 1 GPa. The CPC/PLGA exhibited initial and final setting times of 7 and 12 min, respectively. Although the incorporation of PLGA microspheres increased the force necessary to inject the cement and decreased the percentage of injected mass as function of time, the CPC/PLGA appeared fully injectable at 4 min. Moreover, in comparison with CPC, CPC/PLGA showed a full degradation in 6 weeks (with 100% mass loss) and this was associated with an acidification of the medium containing the CPC/PLGA sample (pH of 3.5 after 6 weeks). A cell viability test validated CPC/PLGA biocompatibility and *in vivo* analyses using a bone defect assay in caudal vertebrae of Wistar rat showed the good opacity of the CPC through the tail and a significant increased degradation the CPC/PLGA cement a month after implantation. In conclusion, this injectable calcium phosphate cement scaffold appears to be an interesting material for bone substitution.

1. INTRODUCTION

The management of metastatic fractures has become a real public health problem[1]. Indeed, the incidence of these bone events is continuously increasing, and their occurrence is causing both morbidity and specific quality of life decrease[2,3]. Traditionally, autologous bone grafts as the "gold standard" in the field have been used to restore damaged bone. However, due to the lack of availability and issues of traditional bone grafts, the use of synthetic biomaterials as bone graft substitutes gained a great interest.

The role of a bone repair scaffold is to provide a suitable 3D architecture and mechanical properties to support bone formation[4,5]. Scaffolds features should be designed and tailored depending on their intended application. For example, for the filling of small bone defects such as vertebral fractures, minimally invasive surgery with injection of biomaterials seems the most appropriate[6]. Percutaneous vertebroplasty consists in stabilizing the fracture using a minimally invasive injection (controlled by radiography or computerized tomography) of a bone cement such as a poly(methyl methacrylate) (PMMA) in the damaged vertebra[6,5]. The use of PMMA which is the gold standard of injectable cement in orthopedics was initiated by Charnley in 1960[7]. However, the polymerization, which is highly exothermic, can causes necrosis and possible residual monomers are associated with risks of cytotoxicity and emboli[8]. Its hardness causes fractures of adjacent vertebrae due to poor load distribution[9]. Moreover, its hydrophobic nature and bio-inertia do not allow good integration into the surrounding bone tissue[10]. Therefore, there is a need for injectable cements able to support new bone tissue formation.

Since the bone mineral phase is a poly-substituted hydroxyapatite , phosphocalcic biomaterials, with a composition comparable to calcified tissues, have been developed[11]. Phosphocalcic ceramics and cements are perfectly biocompatible materials, *i.e.* they facilitate bone reconstruction and a complete recolonization of lesions linked to their progressive resorption[12,13]. Calcium phosphate ceramics are very interesting for their applications in bone

filling and can be found in various forms (granules, dense or porous solid parts, etc.). The main advantage of biomedical cements over bioceramics is their ability to perfectly fill the defect due to their implantation as malleable or injectable pastes.

Calcium phosphate cement (CPC) are hydraulic cements obtained by an acid-base reaction in an aqueous phase between acidic calcium phosphates and more basic calcium phosphates[14]. This setting reaction is generally lightly exothermic, but do not generate as much as heat as the polymerization of MMA in PMMA; thus a significant advantage[15]. Currently, CPC are lacking of osteogenic properties, and that is one of the main driver to develop new formulation (e.g. ion doping) or to incorporate bioactive substances and endogenous cells[16,17]. CPCs are biodegradable more or less quickly with satisfactory mechanical properties. Despite a large number of formulations, CPCs can be classified according to the nature of the product resulting from the setting reaction. This can be either apatite or brushite which is the most thermodynamically stable calcium phosphate at low pH and which will then turn into apatite after in vivo implantation[18–20]. Brushite (slightly acidic) can be obtained for instance by a reaction between β-TCP (almost neutral) and monocalcium phosphate monohydrate, MCPM (acidic)[21]. Injectable CPC must satisfy a number of standards in order to be used in vertebroplasty[22].

In addition to good biocompatibility and compressive strength, suitable properties of the bone cement, such as an adapted viscosity, cohesivity and setting time, should be devised to prevent its leakage and allow excellent adaptation to the most complex cavity shapes. A follow-up with X-ray imaging is mandatory after a vertebroplasty and, as a consequence, the cement must be radio-opaque[23]. A number of additives such as Tantalum oxide, barium sulfate, bismuth and strontium have been proposed to increase radio-opacity of CPCs[24]. More recently, different studies have shown that the use of ZrO_2 is a promising alternative in terms of handling, strength and setting time to synthetize radio-opaque injectable CPC[25,26].

The resorbability of cement generally remains slow, with *in vivo* biodegradation slower than the growth of neoformed bone[27]. To allow vascular and cellular penetration into the heart of the biomaterial before its resorption, an interconnected macroporous structure is an essential condition. CPCs are naturally microporous due to the presence of water from the liquid phase and the acid-base setting reaction. These pores have generally a diameter lower than 5µm and represent 35 to 50% of the cement volume depending on the liquid/powder ratio used to prepare the cement[28]. The size of the macropores must be at least 50 µm[27] (or better 100 µm[29]) and up to 300 µm[30]. The absence of natural macroporosities of a given material explains its low osteoconductivity and limits clinical applications. Several strategies have been implemented to improve the resorbability, including playing on the architecture[31], adding a porous agent[32], or using a phase with a better resorbability, such as calcium sulfate or a metastable calcium carbonate[33]. In recent years, better results have been obtained by introducing composite material as a solution into the liquid phase or into the solid phase (mainly as powder, fibers or microspheres)[34]. Different polymers have been used such as gelatin[35,36], poly(trimethylene carbonate) (PTMC)[37,38] or most commonly poly(lactic-co-glycolide) (PLGA)[39–44].

The objective and originality of this work was to develop an injectable CPC with good opacity and porosity able to support bone formation. We first fabricated brushitic cement with the incorporation of ZrO_2 as a radio-opacifier. The composite nature of CPCs was developed by introducing PLGA microspheres in the cement, with the aim of improving porosity and by consequence the osteoconductivity as well as the resorption rate. The CPC/PLGA was analyzed for several parameters including opacity, handling, and mechanical properties. In vitro degradation and biocompatibility were studied. Finally, the CPC/PLGA was studied in vivo with a model of caudal rat vertebrae. Our results suggested that this innovative brushitic injectable cement doped with ZrO_2/PLGA is a very interesting alternative to PMMA for a use in bone regeneration.

2. EXPERIMENTAL SECTION

2.1. Materials. Poly(D,L-lactide-co-glycolide) (Resomer RG503H), sodium pyrophosphate dibasic ($H_2Na_2O_7P_2$, CAS 7758-16-9), β-tri-calcium phosphate (β-TCP, >98% β-phase basis, CAS 7758-87-4), zirconium(IV) oxide (ZrO_2, 99% trace metals basis, CAS 1314-23-4), citric acid (>99.5%, CAS 77-92-9), 2- propanol (CAS 67-63-0), ethanol (96% vol, CAS 64-17-5), dichloromethane (>99.9% (GC), CAS 75-09-2), phosphate buffered saline (PBS) (P4417) tablets, and 3-(4,5-dimethylthiazol-2-yl)-2,5-diphenyl tetrazolium bromide (MTT, 98%, CAS 298-93-1) were purchased from Sigma-Aldrich. Acetone (≥99% (GC), CAS 67-64-1) and poly(vinyl alcohol)(PVA, CAS 9002-83-5) was purchased from Honeywell. Calcium phosphate monobasic monohydrate, (MPCM, 99%, CAS 10031-30-8) was purchased from STREM chemicals, Inc. MEM alpha medium (Gibco 12571-063), dimethyl sulfoxide (DMSO) (BDH Prolabo 23486.297), foetal bovine serum (FBS) (Eurobio CVFSVF00-01), penicillin/streptomycin (Gibco 15140-122) and 0.05% trypsin-EDTA (Gibco 25300-054) were used for cell cultures.

2.2. Preparation of PLGA microspheres. To prepare PLGA-microspheres of around 100 μm in diameter, a double-emulsion-solvent-evaporation method (water-in-oil-in-water or $W_1/O/W_2$) was used. Microspheres were produced by first dissolving 500 mg of PLGA in 5 ml dichloromethane (DCM), forming oil phase (O). Then 1 mL of distilled water which is the first aqueous phase (W_1) was added to the oil phase. The mixture was emulsified using an Ultra-Turrax emulsifier (T25 digital, IKA) for 90 s at 22000 rpm. Then, 6 mL 0.3% aqueous poly(vinyl alcohol) (PVA) solution (W_2) was added and emulsified for another 90 s at 22000 rpm to produce the second emulsion. After which 394 mL 0.3% (wt/wt) PVA solution and 400 mL 2% 2-propanol solution were added to the mixture. The resultant $W_1/O/W_2$ emulsion was stirred overnight at room temperature to evaporate the solvent and solidify PLGA microspheres.

Then, the microspheres were finally washed in distilled water and collected through centrifugation at 3000 rpm for 10 min, lyophilized and stored at 4°C until use. The size distribution of PLGA microspheres was characterized using a laser diffraction particle size analyzer (Mastersizer 3000).

2.3. Fabrication of CPC/PLGA samples. The MCPM and β-TCP powder were sieved to obtain only 150 and 50 μm particles, respectively. Brushite cement was prepared by mixing MCPM and beta-TCP at 0.45:0.55 ratio (45%:55%, wt/wt), with 20 % (wt/wt) Zirconia and 1% (wt/wt) disodium dihydrogen pyrophosphate. Calcium phosphate cements (CPC) were prepared by addition of citric acid (0.5M) solution, to powder at liquid ratio of 0.4 mL per gram of cement (irrespective or ZrO_2 content). Macroporous cement was fabricated by addition of 30% (wt/wt) of PLGA microsphere to the powder mixture and denoted as CPC/PLGA30. The addition of liquid was adjusted to keep a powder/liquid ratio of 0.4. CPC and CPC/PLGA30 formulations were mixed using a spatula for 1 min in a glass plate and immediately transferred to a 5 mL syringe. After which, the paste was injected in silicon rubber molds of 5 mm diameter and 2 mm height. Within 15 min samples were transferred to calcium free Dulbecco's phosphate buffered saline (DPBS, Sigma) to allow for complete setting at 37°C for 24 h.

2.4. Opacity measurements. For X-ray opacity measurements, 2 mm thick samples were produced. The X-ray opacity was measured at 0.65 mAs, 80 kV using an OBI (On-Board Imager®) (TrueBeam-Stx, Varian). A 2 mm sample of a PMMA-based cement (Vertebroplastic, Biomet, France), which has zirconia as radiopacifier, was used as control along with an aluminum wedge (2–8 mm) in 1 mm steps. The photos were treated with the software Image J to determine the grey level between the samples. All samples were measured in triplicate.

2.5. Morphology analysis. The PLGA microspheres, CPC and CPC/PLGA scaffold morphology, and microstructure were analyzed by scanning electron microscopy (SEM)

(HITACHI S4800 system). Voltage was fixed at 2 KeV. For SEM observation, scaffolds were coated with platinum using a Polaron SC7620 Mini Sputter Coater. Three pictures were taken per samples and 2 samples were analyzed per condition.

2.6. Mechanical properties. The mechanical properties of the CPC and CPC/PLGA30 scaffolds were characterized using a materials testing machine (1/ME) in compression mode coupled with a 5 kN force sensor (MTS). Samples were made by casting the material in silicone molds of cylindrical shape (10 mm in diameter and 20 mm in height). These samples were, then, placed in between dedicated parallel plate jaws and compressed at a constant speed of 0.01 $mm.s^{-1}$ until they broke. During their compression, cylinders were imaged with a 16 Mb camera (SVS-VISTEK) at 1 Hz. In order to perform digital image correlation (DIC) and follow accurately the local displacements on the samples, these latter were initially coated on their surface with a random pattern made of thin black paint droplets. Compression images were then post-processed with dedicated DIC algorithm already presented in former publications[45,46]. The displacement field deduced from DIC were used to deduce the evolution of the sample strain without inaccuracy coming from the machine and jaw plays. Linear elastic regions from the stress−strain graphs were then used to calculate the Young's modulus. These latter were averaged over at least three identical samples. The stress at which the sample begins to break was also measured. All samples were measured with at least n = 5.

2.7. Structural and chemical properties. The X-ray diffraction (XRD) patterns of CPC and CPC/PLGA30 scaffolds were recorded using CuKα radiation, 2Θ range of 10-70° with a scan speed of 2°. min^{-1}, and the PANalytica Xpert powder XRD system. The Fourier Transform Infrared (FTIR) spectrum of CPC and CPC/PLGA30 nanocomposites was recorded with the NEXUS instrument, equipped with an attenuated total reflection accessory in the frequency range of 600−4000 cm^{-1}. The FTIR spectrum was scanned at 1 cm^{-1} resolution, and signals were averaged from 32 scans. Energy-dispersive X-ray spectroscopy analysis (EDX) was taken

with Zeiss EVO ED15 microscope coupled with an Oxford X-MaxN EDX detector. All samples were measured in triplicate.

2.8. Degradation study. For the degradation study, CPC and CPC/PLGA30 samples were placed in 3 ml PBS (pH 7.4) and incubated using an Incu-Shaker (Benchmark) in at 37°C and 70 rpm for 10 weeks. 3 samples were analyzed at each week 1, 2, 4, 6 and 10 of incubation. Immediately after removal of the samples from the incubator, the pH of the PBS medium was measured and the samples were vacuum dried overnight before measuring the mass. Mass change of the samples was calculated using the following equation:

Mass loss (%) = m_0-m_n/m_0 * 100, where mass loss = mass change of sample at t = n (%), m_0 = mass of sample at t = 0 (g), m_n = mass of sample at t = n (g).

2.9. Setting time and injectability. Initial and final setting time was assessed using custom available Gillmore needles (ASTM C266). For this, a plastic mould 10 mm in diameter and 15 mm in height was used as a mould. Samples were mixed and injected into the mould, after which the initial and final setting time was determined. Tests were performed in at least 3 samples. Injectability tests were done on the CPC and CPC/PLGA30 samples in two different methods. Briefly, the first method consists to evaluate by extrusion (i.e., quantification of residual-cement mass retained in the syringe after applying a standard force), during a predetermined injection time period the injectability. Syringes of 10 mL (Omnifix® luer lock solo without needle) were filled with ~ 8 g fresh-cement paste. After predetermined times from the mixing, the cement was extruded manually. The injectability was calculated as: I = [(mi – mf)/mi]×100% where I is the injectability, mi is the initial mass and mf is the final mass of the extrusion. The second method consists to after mixing the powder with liquid, to place the syringe, vertically in a fixture and put under the plates of a handmade injection machine. At a predetermined time of 4 min after mixing the cement, the cement was extruded with a

compression rate of 0.2 $mm.min^{-1}$ up to a maximum force of 100 N. Compressive force was applied to the syringe and recorded as a function of the plunger travel length. All tests were performed in threefold.

2.10. Cell viability assays. Scaffolds were sterilized with ethanol for 30 min and under UV light (405 nm) for 1h as reported in a previous study[47]. Cell response was studied using the MG63 osteoblast-like osteosarcoma cells cultured on the sterilized scaffolds for 7 days. Cell viability was analyzed using the MTT assay. Cells were incubated with 100 µL of culture medium containing 0.05 $mg.\ mL^{-1}$ of MTT solution for 3h. The obtained purple-colored formazan crystals, due to MTT reduction by living cells, were solubilized by addition of 100 µL of DMSO and absorbance recorded at 560 nm using a Multiskan microplate spectrophotometer (Thermofisher, USA). All samples were measured with n =5 in triplicate.

2.11. Implantation in rat vertebrae. Male Wistar rats ((Crl:(Wi)Br), Charles River, France) with weight around 400 g were used for an adequate vertebrae size. The rats were kept in light controlled, air-conditioned rooms and fed ad libitum. A total of 3 vertebrae were used as control (defect which remained empty of materials), 6 vertebrae were used for CPC and 5 for CPC/PLGA30 implantation. The rats were anesthetized with an intraperitoneal injection of ketamine and xylazine (Alcyon, Pau, France) (40 and 9mg/kg, respectively). The tail was disinfected and a dorsal incision was made approximately from Cd31 to Cd35 vertebrae. The skin and the muscles were retracted with buffered saline solution irrigation, the vertebrae were exposed and an intra-osseous defect of 3x3 mm was performed in the exposed surface of the vertebrae. CPC and CPC/PLGA30 were prepared freshly and injected directly after the required setting time to allow the incorporation of the material in each vertebra. After treating the hard tissue, the skin was tightly sutured with resorbable sutures (Vicryl 3/0, Ethicon, Issy les Moulineaux, France). Following surgery, Buprenorphine SR-LAB (Wildlife Pharmaceuticals,

Windsor, CO, USA) was used at a dose of 1.2 mg/kg to provide 72 h analgesia. The wound was controlled daily during the healing period.

2.12. X-ray micro-CT analysis. MicroCT imaging was performed just after implantation and 1 month later using a micro-CT instrument (NanoScan PET-CT, Mediso, Münster, Germany). The rat tails were scanned at 360° rotation at 0.5 degree intervals using a maximum zoom. Image analyses were performed using the 3D reconstruction and analysis 3D Slicer software (https://slicer.org). Different modules were used including Segment Editor and Volumes (with the ColdToHotRainbow lookup table). Regions of interest were defined manually using the Paint module.

2.13. Histological analyses. At the end of the experiment, the rats were sacrificed by decapitation. The tail encompassing Cd32 and Cd35 was harvested. The vertebrae were then fixed in formol during 3 days, decalcified during 10 days in TBD-2 (Thermo Fisher Scientific, France), and included in paraffin. Tissue sections were made (3µm), stained with haemaotoxylin-eosin-safran (HES), scanned using a Nanozoomer Hamamatsu and visualized using the NDPview2 software (https://www.hamamatsu.com). A pathologist performed histological analyses.

3. RESULTS AND DISCUSSION

A CPC doped with ZrO_2 was first obtained by mixing a powder phase (MCPM, β-TCP and ZrO_2) with a solution of 0.5M citric acid. Then PLGA microspheres were added to formulation to obtain macroporous injectable cement.

3.1. Obtention of a radio-opaque CPC

A major concern with vertebroplasties is the risk of cement leakage. The use of an injectable cement requires an imaging monitoring of its injection into vertebrae and therefore using of a

radio-opaque material is essential. To achieve this requirement, different percentages of zirconia were introduced in the CPC formulation. CPC cement were produced using MCPM and β-TCP at a 55 to 45 molar ratio[48]. Figure 1 shows the comparison of the opacity of our ZrO_2-containing CPCs with commercial PMMA cement (Biomet Bone Cement V) and with aluminum sheets used as references.

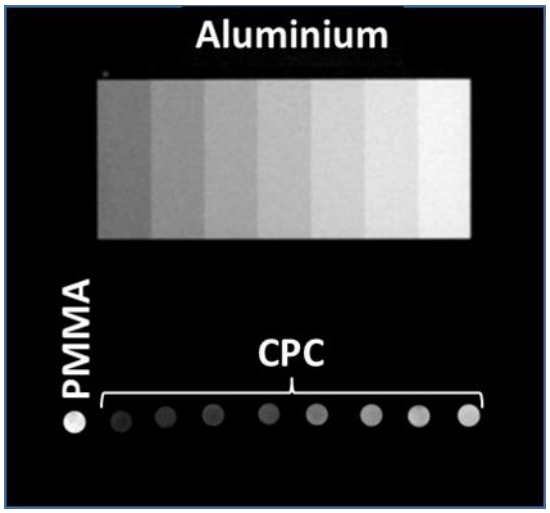

Figure 1. Illustration of cement opacity. Aluminium sheets (from 2 to 8 mm) and commercial PMMA were used as controls. CPC with different ZrO_2 percentages (0, 1, 5, 10, 20, 30, 40 and 50%) were imaged.

Below 20% of ZrO_2, CPC were not visible by radiography meaning that such CPC cannot be used in vertebroplasty. CPC containing 20% ZrO_2 were equivalent to 2 mm of aluminium and clearly visible by X-ray imaging. Intensities of grey level are given in Table 1.

Table 1. Opacity intensities of aluminum sheets, commercial PMMA and different CPCs. The intensity of the samples was obtained in arbitrary unit (a.u.) thanks to the FIJI software.

Samples	Aluminium (2mm)	PMMA	CPC (0%ZrO_2)	CPC (10%ZrO_2)	CPC (20%ZrO_2)	CPC (30%ZrO_2)	CPC (40%ZrO_2)	CPC (50%ZrO_2)
Intensity (a.u.)	48051	54306	44153	46513	48323	50039	51219	52136

In Figure 2, the compression strength and Young's modulus of the samples are given as a function of the ZrO_2 percentage. The influence of zirconia on the mechanical properties was

evaluated on CPC with 20 to 40% of ZrO_2. CPC without zirconia had compression strength of 3MPa; in comparison CPC with 20% ZrO_2 had 23MPa which represent a significant increase. These results could have been expected as a low amount of ZrO2 act as filler in the CPC continuous phase. Nevertheless, this compressive strength improvement obtained by the incorporation of ZrO2 in CPC specially has never been observed in the literature as far as we know. Above 30% of ZrO_2, compression strength decreased by half. The same behavior was observed for Young's modulus, CPC with 20% ZrO_2 had a Young's modulus 7 fold-higher than CPC alone but after 30% the value decreased. The diminution of mechanical properties after a certain content of ZrO_2 was probably due to a change in L/P ratio, which was not optimal anymore, or by the aggregation of ZrO2 in the calcium phosphate. In conclusion, the incorporation of 20% ZrO_2 in the CPC formulation was enough to obtain good radio opacity and, in the same time, a strong increase of the mechanical properties of the cement. From this point and for the rest of the study, the CPC formulation with 20% of ZrO_2 was chosen and will be denoted as CPC.

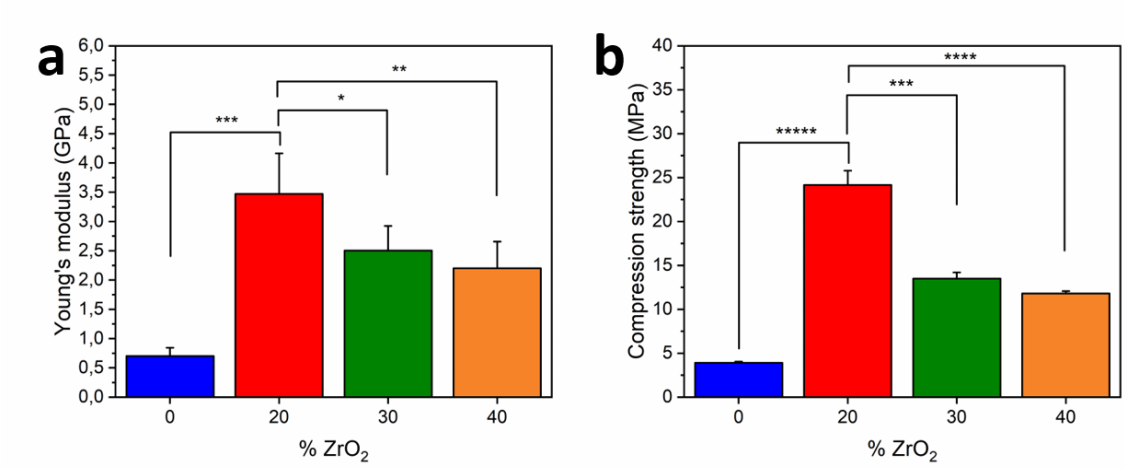

Figure 2. Mechanical properties of the CPCs containing different ZrO_2 concentrations. (a) Compression strength and (b) Young's modulus values. The statistical significance between groups were determined with the Student's t-test and were considered significant for *p < 0.05, **p < 0.005, *** p < 0.0005, **** p < 0.00005 and ***** p < 0.000005.

3.2. Introduction of PLGA microspheres in the CPC

PLGA microspheres were synthesized as described in the Experimental section and observed by SEM as shown in Figure S1. Microspheres had a spherical shape, a smooth surface and homogeneous sizes. This was confirmed by particle size distribution analysis which gave an average size of 133 µm and a polydispersity index of 1.1 (Table S1).

To generate CPC/PLGA scaffold, microspheres at 30% (wt/wt) were added to the CPC and cylindrical blocks were generated. The SEM micrographs showing the inside surface after sectioning cylindrical block of CPC and CPC/PLGA30 are presented in Figure 3a-d. All pictures illustrated the incorporation of the PLGA microspheres. The microspheres were homogeneously spread in the CPC as shown in Figure S2. According to previous studies, interconnected porosity was observed when PLGA microspheres with size above 50 µm were introduced in CPC with a loading of 20%[49]. In Figure 3e and 3f, SEM micrographs showed CPC/PLGA30 after calcination at 600°C for 2 hours which destroyed the PLGA microspheres and generated a CPC with a high porosity. In Figure S3, µCT imaging of the samples after calcination showed an increase of the macroporosity from 3.8% to 44.2% for CPC and CPC/PLGA30, respectively (Table S2 in supporting information). The introduction of macroporosity can accelerate the degradation of the cement as shown in our study. The cement macroporosity can be modulated to obtain enough porosity to allow cell infiltration and proliferation with good mechanical properties, degradation and opacity.

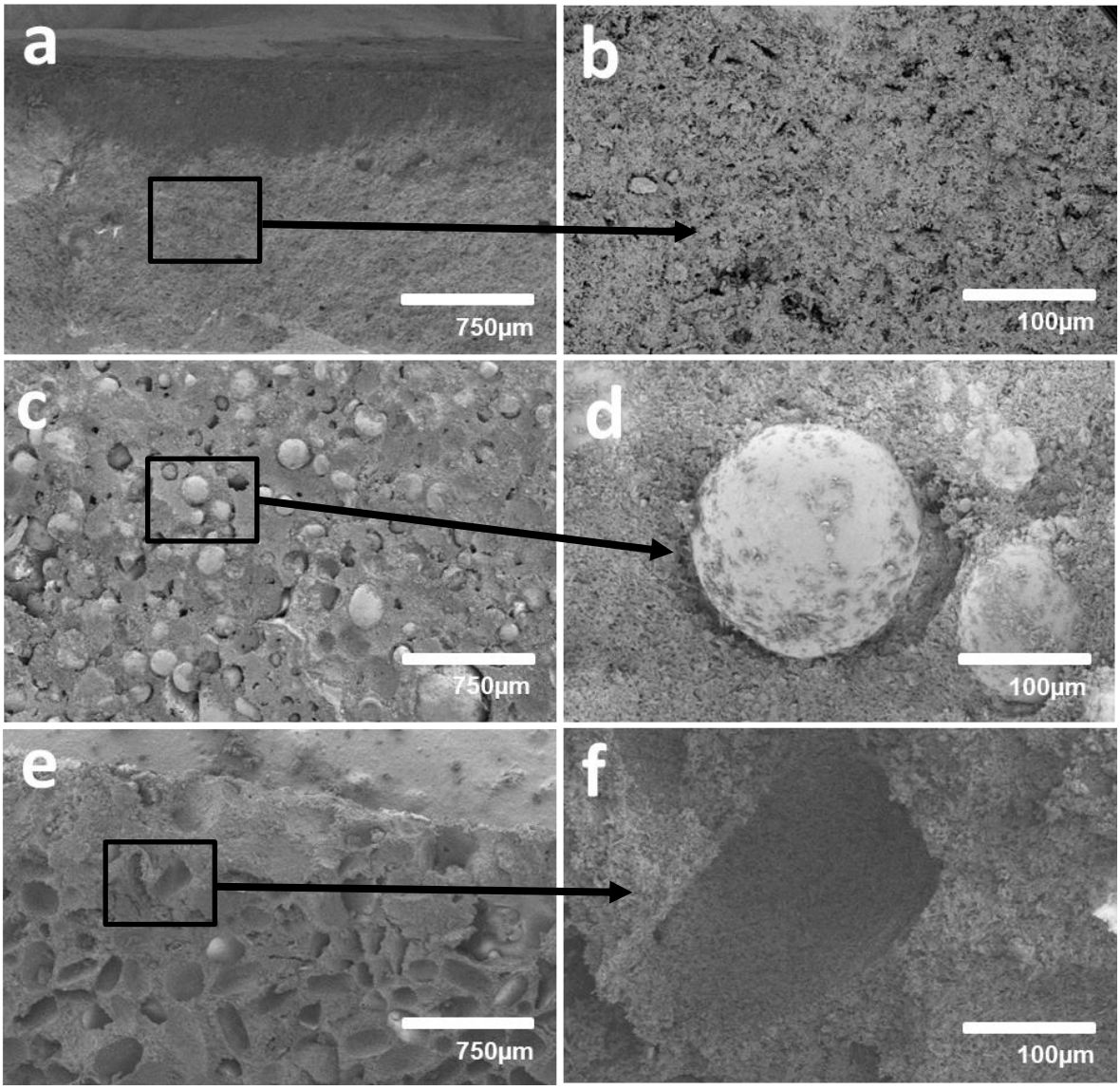

Figure 3. Scanning Electronic Microscopy images of CPC. Images showing sections of CPC (a and b) or CPC/PLGA30 (c and d). SEM images showing surface of CPC/PLGA30 after calcination (e and f).

To confirm brushite formation during the cement preparation, as well ZrO_2 and PLGA incorporation, XRD analysis was performed on the CPC and CPC/PLGA30 cements and data are shown in Figure 4a. The CPC (shown blue) showed five characteristics peaks of brushite phase at $2\theta = 11.6$, 21, 30.5, 31.3 and 30.4° as mentioned by the symbol ●, that described the formation of a unique phase during the cement preparation. The addition of ZrO_2 was demonstrated by the presence of four peaks at $2\theta = 31$, 35, 50 and 60° corresponding to the plan

(111), (200), (220) and (311), respectively (mentioned by ■ in the red diffractogramm). The last diffractogram (black line) showed the presence of one peak at 2θ = 24° mentioned by "*" corresponding to PLGA. The diffractograms of ZrO2, MCPM and β-TCP raw materials are shown as reference in Figure S4.

To understand cement organization and the interactions with ZrO_2 and PLGA microspheres during the cement fabrication, FTIR spectra were recorded (Figure 4b). The powder mixture used to prepare the cement showed characteristics bands of β-TCP at 600 and 1000 cm^{-1}. The addition of ZrO_2 was validated by the band at 750 cm^{-1} (■ in the graph). After initiation of the cement by the addition of the liquid phase, the spectra corresponding to brushite cement appeared with characteristics bands at 1000 cm^{-1}.

These bands (mentioned by ●) are attributed to the stretching mode of P-O and bending mode of O-H. O-H bending mode was also found at 1650 cm^{-1}. The last characteristic band corresponding to the stretching mode of O-H was found at 3500 cm^{-1}. The addition of PLGA microspheres to the cement composition was confirmed by the appearance of a band at 1750 cm^{-1} mentioned by * corresponding to C=O stretching mode. Based on the FTIR characterization we were able to confirm the of ZrO_2 and PLGA during the formation of brushite cement.

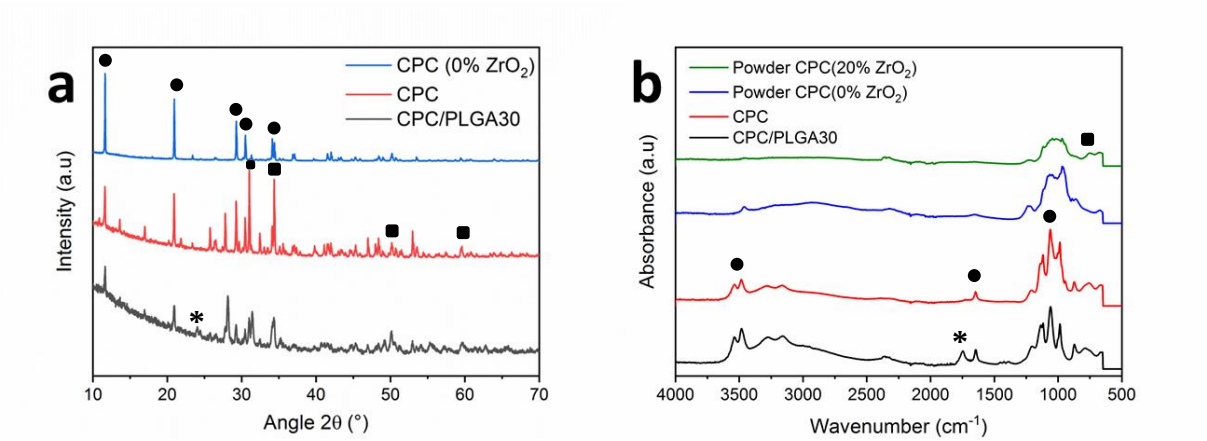

Figure 4. Structural and chemical properties of the CPC and CPC/PLGA cements. (a) Xray-diffractograms of CPC (0% ZrO_2), CPC and CPC/PLGA30 with ●, ■ and * for the characteristics peaks of brushite, ZrO_2 and PLGA respectively. (b) FTIR spectra of CPC powders, CPC and CPC/PLGA cements with ■,● and * for the bands of ZrO_2, brushite and PLGA respectively.

The incorporation of PLGA microspheres modify the structure and have an influence on some properties like opacity (Figure 5). CPC/PLGA30 showed a slight diminution of the opacity but the sample remains still opaque.

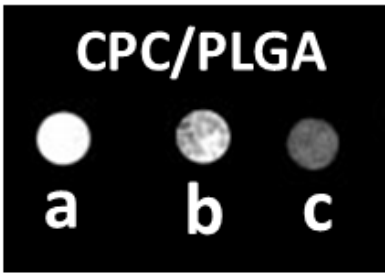

Figure 5. Illustrations of the opacity. (a) CPC with different PLGA percentages (b) CPC/PLGA5 and (c) CPC/PLGA30.

3.3. Mechanical properties, setting times and injectability of the CPC/PLGA

As anticipated, PLGA microspheres addition had an impact on the mechanical properties of CPC as shown in Figure 6. Indeed, the incorporation of 30% PLGA microspheres decreased the compression strength by ten times and the same trend was observed for Young's modulus (from 3.5 to 1 GPa). This diminution of the mechanical properties is in one hand probably due

to the change of the L/P ratio when microspheres were added into the powder phase[50,51]. Indeed the amount of liquid used was higher and could lead to the decrease of the mechanical properties of the cement. Similar results have been already observed in another study[52]. In the other hand, since PLGA has on its own a lower mechanical resistance than the CPC, it could be expected that this lower mechanical strength of the PLGA microparticles would be reflected in the properties of the final cement.

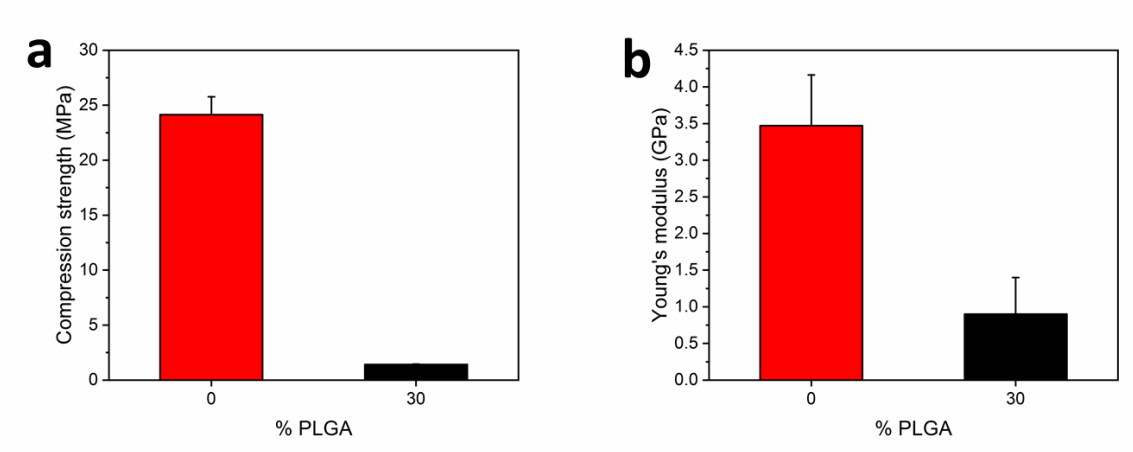

Figure 6. Effect of PLGA microspheres on the mechanical properties of CPC.
(a) Compression strength and (b) Young's modulus values of CPC and CPC/PLGA30.

Important parameters to quantify are the setting time and the injectability of the cement. Indeed, the CPC must to be handling easily by the operator. Figure 7a showed the initial and final setting time of CPC and CPC/PLGA30 pastes. The incorporation of PLGA microspheres decreased the initial setting time from 12 to 7 min. The same effect was observed for final setting time, CPC/PLGA30 showed a final setting time at 12 min while CPC had a final setting time at 22 min. The global diminution of CPC setting time upon addition of PLGA microspheres could be due to a fastest absorption of the liquid by the polymer thus inducing a higher viscosity shortening of the setting time and reduced as well the injectability[40].

The injectability graphs are presented in Figure 7b and 7c. When both pastes were injected at 4 min, almost 100% of the mass was injected. A slight difference between CPC and CPC/PLGA30 was noticed when the pastes were injected at 6 min. By contrast, a significant difference appeared between the samples at 10 min since at that time, CPC was injected at 50% while CPC/PLGA30 was not enough viscous to be injected. The incorporation of PLGA microspheres decreased the injectability after 8 min which is correlated with the setting time. Figure 7c showed the force to inject the paste in function of time (start at 4 min). The graphs showed that the force necessary to inject CPC/PLGA30 is higher until 80 seconds, after which the force reach 100N[53,54] which is the limit of the machine at 100 s.

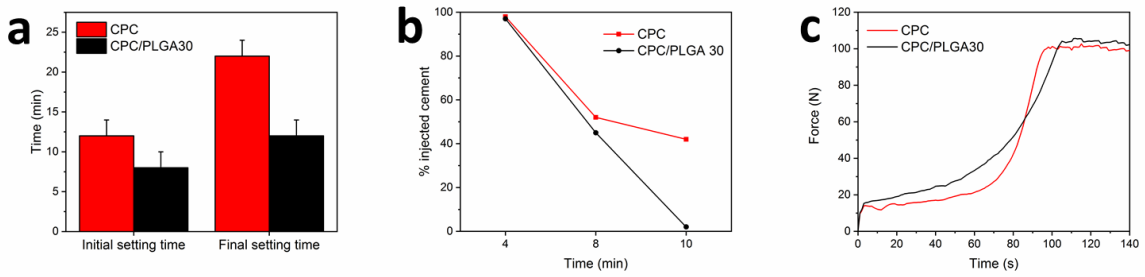

Figure 7. Setting time and injectability of CPC and CPC/PLGA.
a) Initial and final setting times measured using custom available Gillmore needles (ASTM C266), b) Injectability at different time points with hand injection and c) under pressure until 100 N.

3.4. Analysis of the degradation rates of the CPC/PLGA

The influence of PLGA microspheres on the degradation rate of the CPC is an important parameter to quantify. The mass loss of CPC and CPC/PLGA30 as a function of time is given in Figure 8a. The SEM images and the photographs of the cements taken over time confirmed that CPC did not show any significant mass loss even at week 10 (Figure S5). In comparison, mass loss of CPC/PLGA30 after 2 weeks is about 5%. At week 4, CPC/PLGA30 samples showed a high decrease in mass of 70%, indicating PLGA erosion. After 6 weeks, almost all the sample was degraded. The incorporation of 30% of PLGA microspheres in the CPC

formulation leads to an almost complete *in vitro* degradation of the sample after 6 weeks, meaning that the porosity induced by PLGA erosion accelerated the CPC degradation.

The pH of the PBS solution containing CPC and CPC/PLGA30 is given in Figure 7b. The medium of CPC showed a stability of the pH around 7 even after 10 weeks. However, the pH of CPC/PLGA30 showed a high decreased after 2 weeks (pH5 .5), and stabilized from 6 weeks to reach an ultimate pH of 3.5 which is much lower than the pH of CPC. This diminution is due to the hydrolysis of PLGA microspheres that lead to an acidification of the medium.

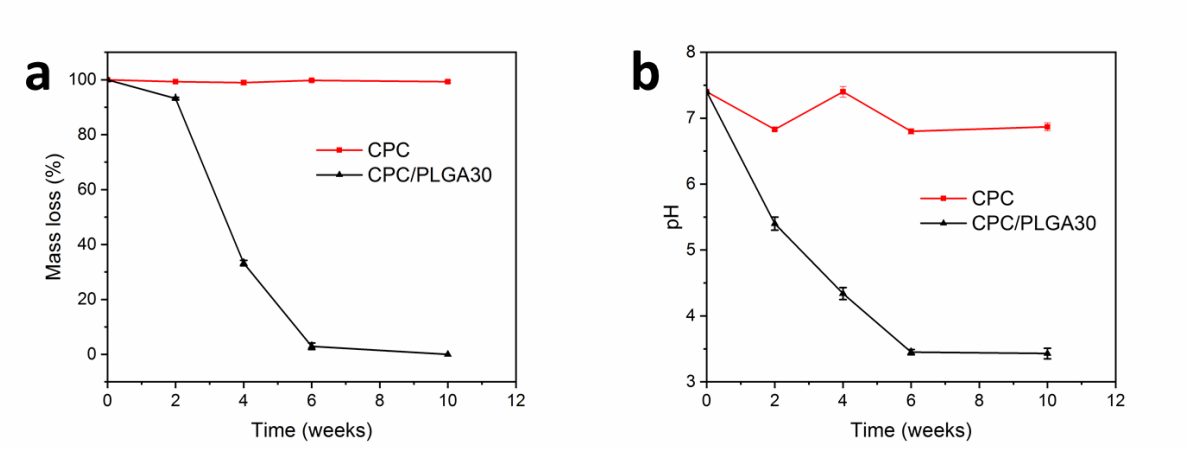

Figure 8. Degradation analysis of the CPC and CPC/PLGA in PBS medium from 0 to 10 weeks.
(a) Percentage of mass loss and (b) medium acidification.

3.5. *In vitro* biological analyses

The biocompatibility of CPC and CPC/PLGA30 was investigated using MG-63 human bone osteosarcoma cells, which have an osteogenic potential. This cellular model has been widely used in the literature as a model to study the effects of biomaterials on human bone cells[55–58]. CPC and CPC/PLGA30 did not induced any significant effect on cell proliferation measured at day 4 and 7 as compared to cells grown without scaffolds (Figure 9). This cell viability test confirmed that CPC and CPC/PLGA30 are biocompatible.

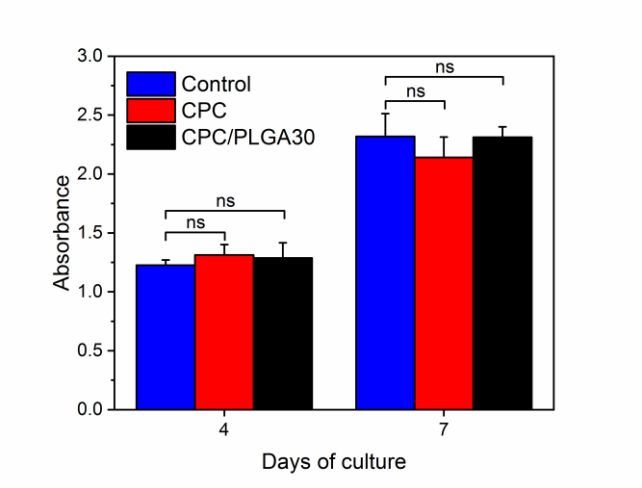

Figure 9. MG-63 cell viability. The cytocompatibility of CPC and CPC/PLGA30 was assessed with the MTT assay at day 4 and 7 after seeding (ns = not significant).

3.6. *In vivo* experiments

In order to confirm the observations obtained *in vitro* concerning the cement degradation, *in vivo* studies on rat caudal vertebrae were performed. Five vertebrae on 4 different rats were used for implantation of CPC or CPC/PLGA30, together with one vertebrae left empty. During the experiments, no infection of the operative site was observed. Figure 10 shows vertebrae reconstruction after *in vivo* micro-CT imaging of the different vertebrae *i.e.* with (Empty) or without (Control) any drill lesion. Vertebrae filled with CPC or CPC/PLGA30 cement are also shown. X-ray images of the same vertebrae show that the opacity of the CPC at the time of implantation is clearly efficient although CPC/PLGA showed a diminution of the opacity due to the incorporation of the PLGA microspheres.

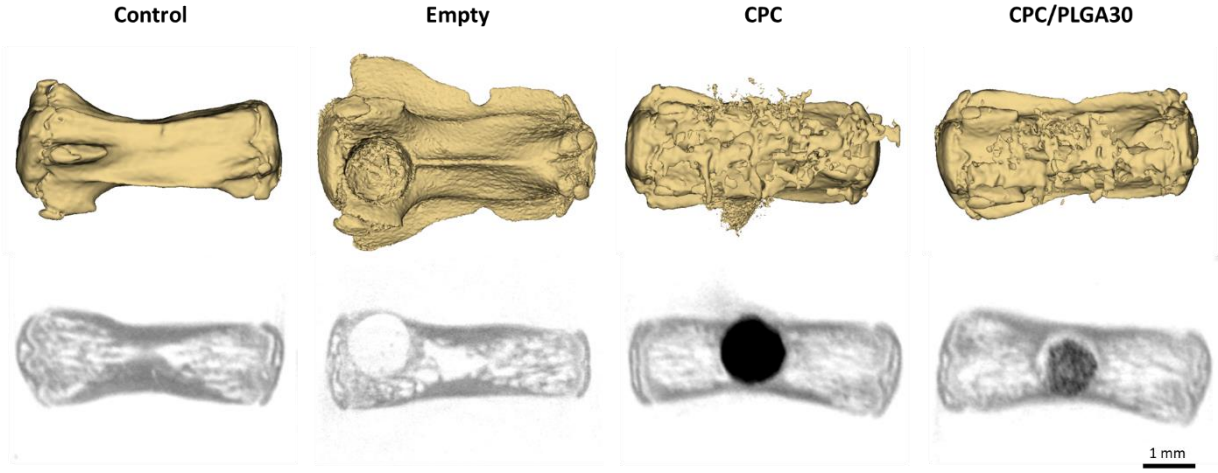

Figure 10. In vivo micro-CT imaging of rat caudal vertebrae with or without cement implantation. Top: MicroCT images (dorsal view) of vertebrae at the time of surgery using the 3DSlicer software (segment editor using a threshold of 2282). The images correspond to vertebrae undrilled (Control), empty or filled with CPC or CPC/PLGA30. Bottom: X-ray images of the same vertebrae as above showing the opacity of the material.

In addition, micro-CT imaging of the cement density at the time of implantation showed that the CPC/PLGA cement is clearly less dense than the CPC one (Figure 11A). This is even better illustrated by the 3D imaging of the two cements, as shown in Figure 11B and C. When using an adapted imaging threshold, CPC appears as a fully compact cement whereas the CPC/PLGA30 imaging shows a highly holed structure generated by the incorporation of the PLGA microspheres.

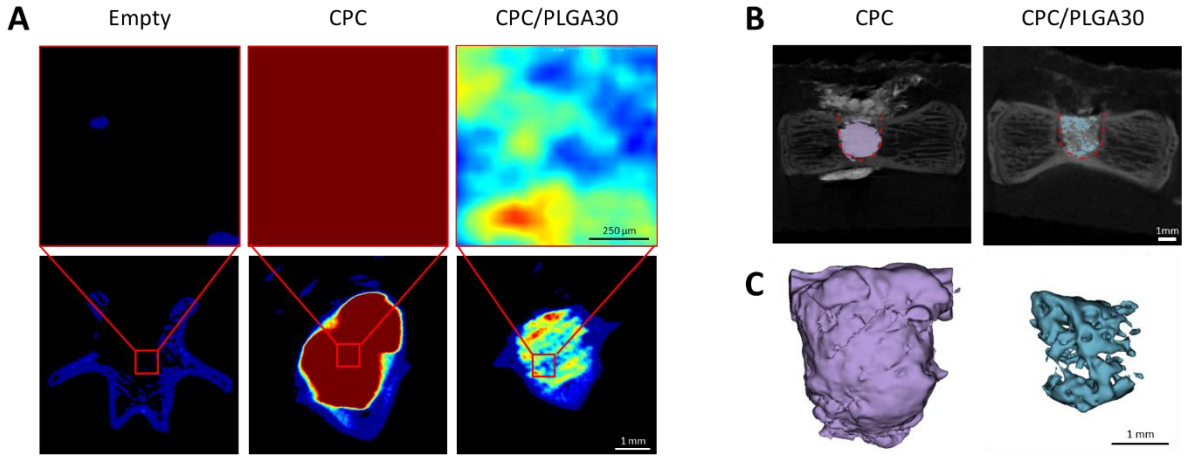

Figure 11. Analysis of cement density by microCT imaging at the time of implantation. A) Images obtained with the 3Dslicer software and a ColdToHotRainbow lookup table showing slices of vertebrae filled with CPC or CPC/PLGA30. Top panel is a 4-fold magnification of the bottom panel). B) MicroCT image of the cements in the vertebrae using the Segment editor module and a threshold of 9647. C) 3D representation of the cement volume from the same vertebrae as in panel B. Bar size showing the magnification used are indicated for each panel.

We then assessed the *in vivo* degradation of the two cements, 1 month after implantation. As shown in Figure 12, we first evaluated the mean density of CPC and CPC/PLGA30 in the corresponding vertebrae, at the time of implantation and one month after (Figure 12A).

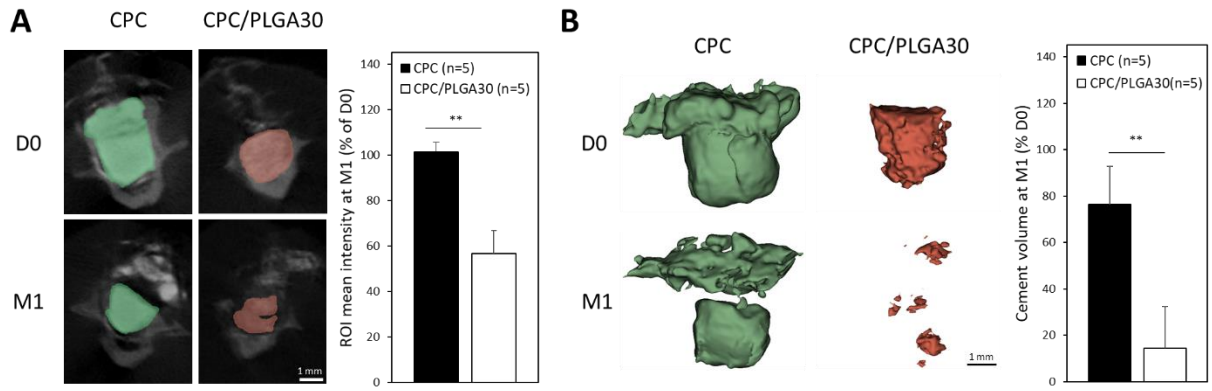

Figure 12. Increased *in vivo* degradation of CPC/PLGA30 as compared to CPC monitored by micro-CT imaging 1 month after implantation. A) Mean intensities of CPC or CPC/PLGA30 sections measured on ROI corresponding to the implanted cement and determined on axial vertebrae sections. Mean intensities are expressed as percent of the value obtained at the time of implantation (D0). B) The volume of the CPC and CPC/PLGA30 cements was measured using the 3DSlicer software (segment editor using a threshold of 7930). Results are as percent of the value obtained at D0. Statistical analysis was performed using the Mann-Whitney test and *p* values are indicated (**<0.01).

Data showed a significant reduction of the density for CPC/PLGA30 as compared to CPC. The Micro-CT imaging also provided a good visualization of the material volume, with a significant difference ($p = 0.008$) between the two materials. Indeed, 1 month after implantation, CPC is still present in the defect with only a slight volume decrease (around 20%), whereas a strong volume reduction of CPC/PLGA30 (more than 80%) is observed 1 month after implantation[59]. Moreover, histological analyses was performed on the vertebrae filled with the two cements. As shown in Supplementary Figure S5, the black material observed in the tail slices probably corresponds to the ZrO2 particles incorporated into the cements. Only very moderate inflammatory reaction was observed and we mainly noticed macrophages eliminating the ZrO2 remaining particles. These observations are supported by previous studies dealing with the biodegradation and biocompatibility of zirconia particles[60,61]. Interestingly, the data confirmed the strong differences in the appearance of the two cements with large holes and more cell infiltration in the CPC/PLGA30 than in the CPC.

4. CONCLUSIONS

In this study, we fabricated a new CPC doped with ZrO_2 and PLGA microspheres. The CPC/PLGA cement was found to have good handling (injectability, initial and final setting time, cohesive properties) and a sufficient radio-opacity. The mechanical strength of CPC was acceptable due to the reinforcement by ZrO_2. This composite has also a good macroporosity and an increased degradability. Indeed, i*n vitro* analysis of CPC/PLGA showed full degradation over 10 weeks, which consequently decreased the pH due to PLGA hydrolysis. The *in vitro* assay with MG63 cells showed the biocompatibility of the material. The *in vivo* study in rat confirmed the opacity and the resorption one month after implantation in caudal vertebrae.

5. Supporting Information. Figure S1. Imaging of PLGA microspheres by SEM; Figure S2. EDX mapping images of atoms elements present in CPC/PLGA30; Figure S3. Micro-tomography images; Figure S4. X-ray diffractograms of raw ZrO_2, MCPM and β-TCP.; Figure S5. Degradation study of CPC and CPC/PLGA over time; Figure S6. Histological images of rat vertebrae; Table S1. Size distribution of PLGA microspheres; Table S2. Porosity and pore size of CPC and CPC/PLGA samples obtained from micro-tomography analyses.

6. ACKNOWLEDGEMENTS

This work/project was publicly funded through ANR (the French National Research Agency) under the "Investissements d'avenir" programme with the reference ANR-16-IDEX-0006. This work was partially supported by the "Région Occitanie" through the project n°20019610 "CoTraitCancer". The RHEM facility (Réseau d'Histologie Expérimentale de Montpellier) was supported by INCa_Inserm_DGOS_12553 (SIRIC Montpellier Cancer), FEDER-FSE 2014-2020 Languedoc Roussillon), IBiSA and the Ligue contre le cancer. We thank Salima Atis, Dr.

Sophie Poty and Dr. Marion Tardieu for the *in vivo* experiments (implantation or imaging analyses). We are also grateful to Dr. Nelly Pirot for support in histological analyses.

7. REFERENCES

1. Amin S.; Achenbach SJ.; Atkinson EJ.; Khosla S.; Melton LJ. Trends in fracture incidence: A population-based study over 20 years. J Bone Miner Res 2014, 29(3):581-589.
2. Oster G.; Lamerato L.; Glass AG.; Richert-Boe KE.; Lopez A.; Chung K.; Richhariya A.; Dodge T.; Wolff GG.; Balakumaran A.; Edelsberg J. Natural history of skeletal-related events in patients with breast, lung, or prostate cancer and metastases to bone: A 15-year study in two large US health systems. Support Care Cancer 2013, 21(12):3279-3286.
3. Weilbaecher, KN.; Guise TA.; McCauley LK. Cancer To Bone: a Fatal Attraction. Nat Rev 2013, 11(6):411-425.
4. Wang W.; Yeung KWK. Bone grafts and biomaterials substitutes for bone defect repair: A review. Bioact Mater 2017, 2(4):224-247.
5. McGraw JK.; Cardella J.; Barr JD.; Mathis JM.; Sanchez O.; Schwartzberg MS.; Swan TL.; Sacks D. Society of Interventional Radiology quality improvement guidelines for percutaneous vertebroplasty. J Vasc Interv Radiol 2003, 14(7):827-831.
6. Nakano M.; Hirano N.; Zukawa M.; Suzuki K.; Hirose J.; Kimura T.; Kawaguchi Y. Vertebroplasty Using Calcium Phosphate Cement for Osteoporotic Vertebral Fractures: Study of Outcomes at a Minimum Follow-up of Two Years. Asian Spine J 2012, 6(1):34.
7. A. Hardinger S.; Wijaya N. A mild method for rapid tert-butyldiphenylsilylation of primary and secondary alcohols. Tetrahedron Lett 1993, 34(24):3821-3824.
8. Lieberman IH.; Togawa D.; Kayanja MM. Vertebroplasty and kyphoplasty: filler materials. Spine J 2005, 5(6):S305-S316.
9. Boger A.; Heini P.; Windolf M.; Schneider E. Adjacent vertebral failure after vertebroplasty: a biomechanical study of low-modulus PMMA cement. Eur Spine J 2007, 16(12):2118-2125.
10. Quan R.; Ni Y.; Zhang L.; Xu J.; Zheng X.; Yang D. Short- and long-term effects of vertebroplastic bone cement on cancellous bone. J Mech Behav Biomed Mater 2014, 35:102-110.
11. Cuisinier Fjg.; J-F. Schaaf.; P. Van Labduyt.; D. Rothi.; J. Lemaître. Immediate implant placement using injectable. J Appl Biomater Biomech 2004, 88-95.
12. Nguyen LH.; Annabi N.; Nikkhah .; Bae H.; Binan L.; Park S.; Kang Y.; Yang Y.; Khademhosseini A. Vascularized bone tissue engineering: approaches for potential improvement. Tissue Eng Part B Rev 2012, 18(5):363-382.
13. Saijo H.; Igawa K.; Kanno Y.; Mori Y.; Kondo K.; Shimizu K.; Suzuki S.; Chikazu D.; Iino M.. Anzai M.; Sasaki N.; Chung UI.; Takato T. Maxillofacial reconstruction using custom-made artificial bones fabricated by inkjet printing technology. J Artif Organs 2009, 12(3):200-205.
14. Ginebra M.; Canal C.; Pastorino D.; Montufar EB. Calcium phosphate cements as drug delivery materials. Adv Drug Deliv Rev 2012, 64(12):1090-1110.
15. Passuti N.; Gouin F. Antibiotic-loaded bone cement in orthopedic surgery. Joint Bone Spine 2003, 70(3):169-174.
16. Shi H.; Ye X.; Zhang J.; Ye J. Enhanced Osteogenesis of Injectable Calcium Phosphate Bone Cement Mediated by Loading Chondroitin Sulfate. ACS Biomater Sci Eng 2019, 5(1):262-271.
17. Shi H.; Ye X.; He F.; Ye J. Improving osteogenesis of calcium phosphate bone cement by incorporating with lysine: An in vitro study. Colloids Surfaces B Biointerfaces 2019, 177:462-469.
18. Brown PW.; Fulmer M. Kinetics of Hydroxyapatite Formation at Low Temperature. J Am Ceram Soc 1991, 74(5):934-940.
19. Apelt D.; Theiss F.; El-Warrak AO.; Zlinszky K.; Bettschart-Wolfisberger R.; Bohner M.; Matter S.; Auer JA.; Von Rechenberg B. In vivo behavior of three different injectable hydraulic calcium phosphate cements. Biomaterials 2004, 25(7-8):1439-1451.
20. Constantz BR.; Barr BM.; Ison IC.; Fulmer MT.; Baker J.; McKinney L.; Goodman SB.; Gunasekaren S.; Delaney DC.; Ross J.; Poser RD. Histological, chemical, and crystallographic analysis of four calcium phosphate cements in different rabbit osseous sites. J Biomed Mater Res 1998, 43(4):451-461.
21. Dorozhkin S V. Self-setting calcium orthophosphate formulations. J Funct Biomater. 2013;4(4):209-311.
22. Lewis G. Injectable bone cements for use in vertebroplasty and kyphoplasty: State-of-the-art review. J Biomed Mater Res Part B Appl Biomater 2006, 76B(2):456-468.

23. Ginebra, M. P.; Albuixech, L.; Fernández-Barragán, E.; Aparicio, C.; Gil, F. J.; San Román, J.; Vázquez, B.; Planell, J. A.Mechanical performance of acrylic bone cements containing different radiopacifying agents. Biomaterials 2002, 23(8):1873-1882.
24. Hoekstra JWM.; Van Den Beucken JJJP.; Leeuwenburgh SCG.; Bronkhorst EM.; Meijer GJ.; Jansen JA. Tantalum oxide and barium sulfate as radiopacifiers in injectable calcium phosphate-poly(lactic-co-glycolic acid) cements for monitoring in vivo degradation. J Biomed Mater Res - Part A 2014, 102(1):141-149.
25. Aberg J.; Pankotai E.; Hulsart Billström G.; Weszl M.; Larsson S.; Forster-Horváth C.; Lacza Z, Engqvist H. In vivo evaluation of an injectable premixed radiopaque calcium phosphate cement. Int J Biomater 2011, 2011:232574.
26. Aberg J.; Henriksson HB.; Engqvist H.; Palmquist A.; Brantsing C.; Lindahl A.; Thomsen P.; Brisby H. Biocompatibility and resorption of a radiopaque premixed calcium phosphate cement. J Biomed Mater Res - Part A 2012, 100 A(5):1269-1278.
27. Bohner M. Design of ceramic-based cements and putties for bone graft substitution. Eur Cell Mater 2010, 20:1-12.
28. Espanol M.; Perez RA.; Montufar EB.; Marichal C.; Sacco A.; Ginebra MP. Intrinsic porosity of calcium phosphate cements and its significance for drug delivery and tissue engineering applications. Acta Biomater 2009, 5(7):2752-2762.
29. Takagi S.; Chow LC. Formation of macropores in calcium phosphate cement implants. J Mater Sci Mater Med 2001, 12(2):135-139.
30. Karageorgiou V.; Kaplan D. Porosity of 3D biomaterial scaffolds and osteogenesis. Biomaterials 2005, 26(27):5474-5491.
31. Ginebra MP.; Espanol M.; Montufar EB.; Perez RA.; Mestres G. New processing approaches in calcium phosphate cements and their applications in regenerative medicine. Acta Biomater 2010, 6(8):2863-2873.
32. Lodoso-Torrecilla I.; Van den Beucken JJJP.; Jansen JA. Calcium phosphate cements: Optimization toward biodegradability. Acta Biomater 2021, 119:1-12.
33. Combes C.; Bareille R.; Rey C. Calcium carbonate–calcium phosphate mixed cement compositions for bone reconstruction. J Biomed Mater Res Part A 2006, 79A(2):318-328.
34. De Lacerda Schickert S.; Pinto JC.; Jansen J.; Leeuwenburgh SCG.; Van Den Beucken JJJP. Tough and injectable fiber reinforced calcium phosphate cement as an alternative to polymethylmethacrylate cement for vertebral augmentation: A biomechanical study. Biomater Sci 2020, 8(15):4239-4250.
35. Habraken WJEM.; de Jonge LT.; Wolke JGC.; Yubao L.; Mikos AG.; Jansen JA. Introduction of gelatin microspheres into an injectable calcium phosphate cement. J Biomed Mater Res Part A 2008, 87A(3):643-655.
36. Li M.; Liu X.; Liu X.; Ge B.; Chen K. Creation of macroporous calcium phosphate cements as bone substitutes by using genipin-crosslinked gelatin microspheres. J Mater Sci Mater Med 2009, 20(4):925-934.
37. Habraken WJ.; Zhang Z.; Wolke JG.; Grijpma DW.; Mikos AG.; Feijen J.; Jansen JA. Introduction of enzymatically degradable poly(trimethylene carbonate) microspheres into an injectable calcium phosphate cement. Biomaterials 2008, 29(16):2464-2476.
38. Liao H.; Walboomers XF.; Habraken WJ.; Zhang Z.; Li Y.; Grijpma DW.; Mikos AG.; Wolke JG.; Jansen JA. Injectable calcium phosphate cement with PLGA, gelatin and PTMC microspheres in a rabbit femoral defect. Acta Biomater 2011, 7(4):1752-1759.
39. Simon CG.; Khatri CA.; Wight SA.; Wang FW. Preliminary report on the biocompatibility of a moldable, resorbable, composite bone graft consisting of calcium phosphate cement and poly(lactide-co-glycolide) microspheres. J Orthop Res 2002, 20(3):473-482.
40. Qi X.; Ye J. Mechanical and rheological properties and injectability of calcium phosphate cement containing poly (lactic-co-glycolic acid) microspheres. Mater Sci Eng C 2009, 29(6):1901-1906.
41. Qi X.; Ye J.; Wang Y. Improved injectability and in vitro degradation of a calcium phosphate cement containing poly(lactide-co-glycolide) microspheres. Acta Biomater 2008, 4(6):1837-1845.
42. Fei Z.; Hu Y.; Wu D.; Wu H.; Lu R.; Bai J.; Song H. Preparation and property of a novel bone graft composite consisting of rhBMP-2 loaded PLGA microspheres and calcium phosphate cement. J Mater Sci Mater Med 2008, 19(3):1109-1116.
43. Schnieders J.; Gbureck U.; Thull R.; Kissel T. Controlled release of gentamicin from calcium phosphate—poly(lactic acid-co-glycolic acid) composite bone cement. Biomaterials 2006, 27(23):4239-4249.
44. Ruhé PQ.; Hedberg-Dirk EL.; Padron NT.; Spauwen PHM.; Jansen JA.; Mikos AG. Porous Poly(DL-lactic- co -glycolic acid)/Calcium Phosphate Cement Composite for Reconstruction of Bone Defects. Tissue Eng 2006, 12(4):789-800.
45. Vu T-L.; Barés J. Soft grain compression: beyond the jamming point 2019, 100 (4), pp.042907.

46. Vu TL.; Barés J.; Mora S.; Nezamabadi S. Deformation Field in Diametrically Loaded Soft Cylinders. Exp Mech 2019, 59:453–46 .
47. Belaid H.; Nagarajan S.; Teyssier C.; Barou C.; Barés J.; Balme S.; Garay H.; Huon V.; Cornu D.; Cavaillès V.; Bechelany M.Development of new biocompatible 3D printed graphene oxide-based scaffolds. Mater Sci Eng C 2020, 110:110595.
48. Sládková M.; Palmer M.; Öhman C.; Alhaddad R.J.; Esmael A.; Engqvist H.; De Peppo G.M. Fabrication of macroporous cement scaffolds using PEG particles: In vitro evaluation with induced pluripotent stem cell-derived mesenchymal progenitors. Mater Sci Eng C 2016, 69:640-652.
49. Link DP.; Van den Dolder J.; Van den Beucken JJ.; Cuijpers VM.; Wolke JG.; Mikos AG.; Jansen JA.Evaluation of the biocompatibility of calcium phosphate cement/PLGA microparticle composites. J Biomed Mater Res A 2008, 87(3):760-769.
50. Engstrand J.; Persson C.; Engqvist H. The effect of composition on mechanical properties of brushite cements. J Mech Behav Biomed Mater 2014, 29:81-90.
51. Jang JH.; Shin S.; Kim HJ.; Jeong J.; Jin HE.; Desai MS.; Lee SW.; Kim SY. Improvement of physical properties of calcium phosphate cement by elastin-like polypeptide supplementation. Sci Reports 2018, 81. 2018;8(1):1-11.
52. Habraken WJEM.; Wolke JGC.; Mikos AG.; Jansen JA. PLGA microsphere/calcium phosphate cement composites for tissue engineering: In vitro release and degradation characteristics. J Biomater Sci Polym Ed 2008, 19(9):1171-1188.
53. Khairoun I.; Boltong MG.; Driessens FCM.; Planell JA. Some factors controlling the injectability of calcium phosphate bone cements. J Mater Sci Mater Med 1998, 9(8):425-428.
54. Dunne N.; O'Gara R.; Buchanan F.; Orr J. Effect of Liquid/Powder Ratio on the Setting, Handling and Mechanical Properties of Collagen–Apatitic Cements. Key Eng Mater 2012, 493-494:415-421.
55. Attik GN.; Villat C.; Hallay F.; Pradelle-Plasse N.; Bonnet H.; Moreau K.; Colon P.; Grosgogeat B. In vitro biocompatibility of a dentine substitute cement on human MG63 osteoblasts cells: Biodentine™ versus MTA®. Int Endod J 2014, 47(12):1133-1141.
56. Wang Y.; Zhang S.; Zeng X.; Ma LL.; Weng W.; Yan W.; Qian M. Osteoblastic cell response on fluoridated hydroxyapatite coatings. Acta Biomater 2007, 3(2):191-197.
57. Di Palma F.; Douet M.; Boachon C.; Guignandon A.; Peyroche S.; Forest B.; Alexandre C.; Chamson A.; Rattner A. Physiological strains induce differentiation in human osteoblasts cultured on orthopaedic biomaterial. Biomaterials 2003, 24(18):3139-3151.
58. Chang YY.; Huang HL.; Chen YC.; Hsu JT.; Shieh TM.; Tsai MT. Biological characteristics of the MG-63 human osteosarcoma cells on composite tantalum carbide/amorphous carbon films. PLoS One 2014, 9(4):1-7.
59. Link DP.; Van den Dolder J.; Jurgens WJFM.; Wolke JGC.; Jansen JA. Mechanical evaluation of implanted calcium phosphate cement incorporated with PLGA microparticles. Biomaterials 2006, 27(28):4941-4947.
60. Sindilar E-V.; Munteanu C.; Aurelian Pasca S.; Mihai I, Henea ME.; Istrate B. Long Term Evaluation of Biodegradation and Biocompatibility In-Vivo the Mg-0.5Ca-xZr Alloys in Rats. Crystals 2021, 11(1):54.
61. Yang Y.; Bao H.; Chai Q.; Wang Z.; Sun Z.; Fu C.; Liu Z.; Liu Z.; Meng X.; Liu T. Toxicity, biodistribution and oxidative damage caused by zirconia nanoparticles after intravenous injection. Int J Nanomedicine 2019, 14:5175.

Graphic for manuscript